AFRL-AFOSR-VA-TR-2017-0072

Unified first-principle analysis of ultraintense laser-matter interactions: Theory, computation and Experiments

Pavel Polynkin
ARIZONA UNIV BOARD OF REGENTS TUCSON
888 N. EUCLID AVENUE
TUCSON, AZ 85722-3308

03/29/2017
Final Report

Air Force Research Laboratory
AF Office Of Scientific Research (AFOSR)/RTB1

REPORT DOCUMENTATION PAGE

Form Approved
OMB No. 0704-0188

1. REPORT DATE *(DD-MM-YYYY)*	2. REPORT TYPE	3. DATES COVERED *(From - To)*
29-03-2017	Final Performance	30 Sep 2012 to 30 Nov 2016

4. TITLE AND SUBTITLE
Unified first-principle analysis of ultraintense laser-matter interactions: Theory, computation and Experiments

5a. CONTRACT NUMBER

5b. GRANT NUMBER
FA9550-12-1-0482

5c. PROGRAM ELEMENT NUMBER
61102F

6. AUTHOR(S)
Pavel Polynkin

5d. PROJECT NUMBER

5e. TASK NUMBER

5f. WORK UNIT NUMBER

7. PERFORMING ORGANIZATION NAME(S) AND ADDRESS(ES)
ARIZONA UNIV BOARD OF REGENTS TUCSON
888 N. EUCLID AVENUE
TUCSON, AZ 85722-3308 US

8. PERFORMING ORGANIZATION REPORT NUMBER

9. SPONSORING/MONITORING AGENCY NAME(S) AND ADDRESS(ES)
AF Office of Scientific Research
875 N. Randolph St. Room 3112
Arlington, VA 22203

10. SPONSOR/MONITOR'S ACRONYM(S)
AFRL/AFOSR RTB1

11. SPONSOR/MONITOR'S REPORT NUMBER(S)
AFRL-AFOSR-VA-TR-2017-0072

12. DISTRIBUTION/AVAILABILITY STATEMENT
DISTRIBUTION A: Distribution approved for public release.

13. SUPPLEMENTARY NOTES

14. ABSTRACT
The focus of this Basic Research Initiative has been on the fundamental aspects of ultrafast laser-matter interactions that are involved in femtosecond laser micromachining. The main scientific results of the program are as follows:
1. We have introduced a new universal criterion of femtosecond laser ablation that is independent on the angle of incidence and polarization of the laser beam.
2. We have conducted experiments on laser-driven microexplosions in sapphire and on the interface of silicon and fused silica. We have discovered several new super-dense phases of aluminum and silicon.
3. We have quantified different ionization channels in femtosecond laser ablation and devised an improved rate equation for ionization for several technologically important transparent dielectrics (sapphire, fused silica, soda-lime glass).

15. SUBJECT TERMS
laser solid interactions, ablation, high intensity

16. SECURITY CLASSIFICATION OF:			17. LIMITATION OF ABSTRACT	18. NUMBER OF PAGES	19a. NAME OF RESPONSIBLE PERSON
a. REPORT	b. ABSTRACT	c. THIS PAGE			PARRA, ENRIQUE
Unclassified	Unclassified	Unclassified	UU		

Standard Form 298 (Rev. 8/98)
Prescribed by ANSI Std. Z39.18

				19b. TELEPHONE NUMBER *(Include area code)* 703-696-8571

I. Summary: The focus of this Basic Research Initiative has been on the fundamental aspects of ultrafast laser-matter interactions that are involved in femtosecond laser micromachining. The main scientific results of the program are as follows:

1. We have introduced a new universal criterion of femtosecond laser ablation that is independent on the angle of incidence and polarization of the laser beam.
2. We have conducted experiments on laser-driven microexplosions in sapphire and on the interface of silicon and fused silica. We have discovered several new super-dense phases of aluminum and silicon.
3. We have quantified different ionization channels in femtosecond laser ablation and devised an improved rate equation for ionization for several technologically important transparent dielectrics (sapphire, fused silica, soda-lime glass).
4. We have developed a new, first-principle, non-paraxial model of optical energy deposition inside transparent dielectrics.
5. We have conducted a detailed investigation of beam and pulse shaping effects in femtosecond laser ablation. We have combined Simultaneous Spatial and Temporal (SSTF) beam focusing with conventional beam shaping (vortex beams) that allowed us to produce complex ablation patterns inside transparent materials.
6. We have conducted several related investigations on the general subject of the interaction of intense laser fields with matter.

The results of research supported by this program have been reported in 31 peer-reviewed publications and numerous invited, plenary, post-deadline and contributed talks at international conferences. Our publications under this program include 3 papers in PRL, 1 paper in Nature Photonics, and 2 papers in Nature Communications. We are currently in the process of finishing up and preparing for submission three more publications. In this report, we discuss the project and its main scientific outcomes.

I. Programmatics:

1. The program involved change of subcontractors. After year 1, it became evident that the main interests of the Colorado School of Mines group are in applications of femtosecond laser micromachining, while this program's focus has been on the fundamental aspects of femtosecond laser-matter interactions. The CSM group has requested to be removed from the program. The freed funds have been put into the support of two new subcontractors: the group of M. Ivanov at the Max Born Institute Berlin and the group of M. Kovacev at the Leibniz Universitat Hannover. These additions have significantly strengthened our team, as evidenced by the high quality publications by those groups that acknowledge the support from this program.
2. The program involved a one-year no-cost extension to support the continuation of the work by the University of Arizona group for one more year. The justification for this extension has been that the tasks originally assigned to the Colorado group (mainly beam and pulse shaping) have been transferred to the Arizona group.
3. The Arizona PhD student Weibo Cheng has accepted a position at Apple Computer in Cupertino, CA and has left Arizona about nine months ago. By the time of his departure we have completed collecting data in our experiments. However, his departure delayed the analysis and publication of these results. Weibo Cheng is currently on leave from the University of Arizona, doing practical training at Apple. His work at Apple is on advanced hardware development. It involves the application of beam shaping techniques to laser micromachining and is directly related to his PhD work under the support from this BRI program. In addition to his work at Apple he is currently preparing his PhD dissertation and finishing up the submission of three research papers on the topics of this BRI. He is expected to graduate from the University of Arizona in 2017.

II. Summary of results:

For the most part, the program tasks have been completed according to the original plan outlined in our proposal. We have developed and applied new computational models for the first-principle description of laser-matter interactions, conducted extensive pump-probe investigations of ultrafast processes involved in femtosecond laser ablation, explored the effects of beam and pulse shaping in laser micromachining and investigated new super-dense material phases that are produced through confined laser-driven microexplosions in sapphire and silicon. It should be noted that two tasks have not been completed: The generation of ultrafast femtosecond X-ray probe for imaging of ionization and the development and release of a shareware version of our numerical code. These tasks have not been completed because our team did not have enough man power and time for that. As quite usual for programs of this duration and magnitude, several research projects not originally planned have been conducted, such as the investigation of realistic bandgap structures in ionization of solid-state materials by the Berlin group. This work has implications in advanced predictive modeling of femtosecond laser ablation.

In what follows, we will briefly discuss our main scientific results.

1. **Universal criterion of femtosecond laser ablation.**

We have conducted extensive investigations of the dependence of ablation threshold, for various materials, on the angle of incidence and polarization of the laser beam. Our findings allowed us to formulate a new universal definition of ablation threshold with oblique illumination. Using the constant, linear value of the index of refraction, we calculate the laser fluence transmitted through the air-material interface at the point of ablation threshold. Our data show that, in spite of the highly nonlinear ionization dynamics involved in the ablation process, the so defined transmitted threshold fluence is universally independent of the angle of incidence and polarization of the laser beam for three dissimilar material types: a dielectric, a metal and a semiconductor. An example of data for ablation threshold fluence for gold is shown in Figure 1. It is evident that the ablation threshold fluence strongly depends on the angle of incidence of the laser beam and polarization. However, the value of internal fluence (immediately under the material surface), *calculated linearly*, as if the reflective properties of the material were not transiently affected by the interaction with the laser pulse, is remarkably independent of both angle of incidence and polarization. The data is qualitatively the same for two other material types that we investigated (a semiconductor – silicon and a transparent dielectric – soda-lime glass).

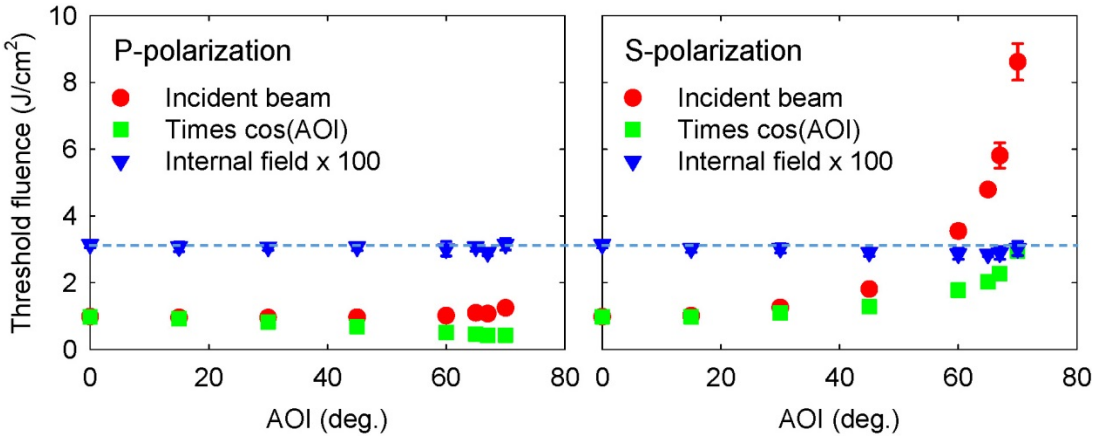

Figure 1: Dependence of ablation threshold fluence on the angle of incidence on a gold sample, for two different polarization of the laser beam (P and S). The value of internal fluence at the point of ablation threshold is independent of the angle of incidence.

We have suggested that the dependence of ablation threshold fluence on the angle of incidence on the sample can be used for accurate measurements of fluence distributions in intense laser beams in air, e. g. in the beams propagating in the filamentation regime. To demonstrate this new measurement approach, we have used ablation of gold samples, at various angles of incidence, to quantify peak clamped fluence in femtosecond laser filaments in air, at different focusing conditions. The result is shown in Figure 2. It is evident from the data that peak fluence strongly depends on external beam focusing. For very lose focusing at 800 nm wavelength, the peak fluence is in the order of 50 TW/cm^2.

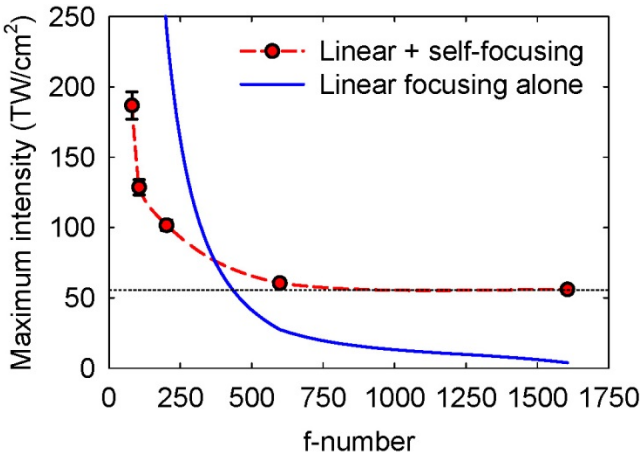

Figure 2: Data for the maximum on-axis intensity along the propagation path, as a function of the f-number of the linear focusing optic, for an 800 nm filament in air. The results of a calculation of the peak intensity for a 2 mJ, 47 fs pulse in vacuum are shown with a solid line.

2. **New material phases of silicon through laser-driven microexplosions.**

The major focus of our program was on the investigations of laser-matter interactions inside transparent materials, e. g. sapphire. Our investigations involved theory, modeling and experiments. The major milestone of this work was the discovery of new material phases of silicon.

Diverse material structures can spontaneously self-organize during cooling from the hot, extremely dense plasma composed of a completely disordered mixture of elements far from thermodynamic equilibrium. Such new structures occur as the randomised atomic configuration within the laser-produced plasma cools down isochorically to ambient temperature, with a very rapid quenching rate of up to 10^{14} K/s. These conditions facilitate the production of metastable end phases that are not energetically accessible through any other experimental means. In this program, we have extended earlier experiments on confined microexplosions inside transparent dielectric materials, by the team members from Australian National University, to the cases of explosions on interfaces between transparent and opaque solids. In this configuration, the microexplosion-based approach becomes applicable to a wide range of materials such as semiconductors, metals and opaque oxides.

We have succeeded in encapsulating novel phases of silicon by creating a laser-driven confined microexplosion on an interface between a layer of transparent silicon dioxide on top of a crystalline silicon substrate. In the regions affected by the microexplosion, we observed at least three metastable tetragonal polymorphs of silicon, two of which have been theoretically predicted in 2008 and 2013 but have never been previously observed in nature or in laboratory experiments. The third observed tetragonal phase has been previously reported in 1986. Furthermore, results of our electron diffraction measurements also indicate the production of at least one additional silicon phase that we cannot ascribe to any of the earlier observed or predicted phases. The discovery of these new material phases has been through electron diffraction techniques. Two examples of BT8 and ST12 phases of silicon are shown in Figures 3 (left and right parts of the figure, respectively).

It has been theoretically predicted that these new phases may exhibit interesting properties, such as low-bandgap semi-conducing (phase BT8) and potentially superconducting (phase ST12) behaviour. The microexplosion technique that we use is capable of producing ordered volumes of these new materials in patterned arrays within the bulk. That would allow for the exploitation of possible unusual properties of these novel materials. The significance of this work is that it opens up the way towards the formation of new classes of materials that are metastable at ambient temperature and pressure, and that may possess novel and useful electronic and physical properties.

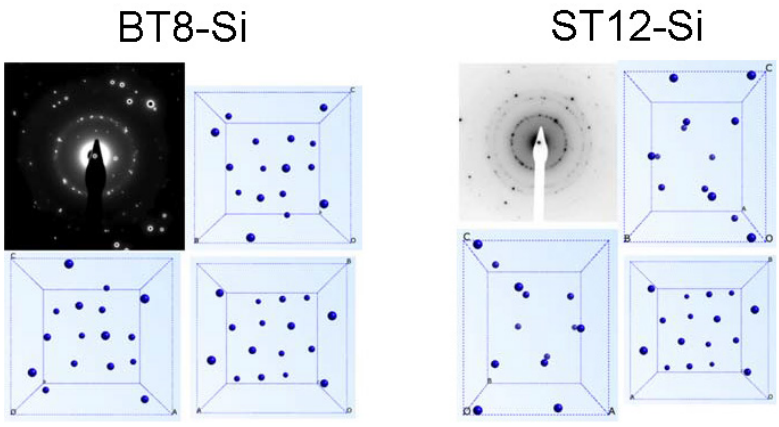

Figure 3, Left: Electron diffraction pattern of BT8-Si, a high-density phase of silicon discovered in our microexplosion experiments. Also shown are the positions of atoms in the 16-atom elementary cell first predicted to exist very recently by J.-T. Wang et al., Phys. Rev. Lett. **110**, 165503 (2013), and calculated using CASTEP, a robust first-principle code based on plane waves and pseudopotentials. Right: Same for the ST12, a high-density phase of silicon discovered in our microexplosion experiments. Also shown are the positions of atoms in the 12-atom elementary cell first predicted to exist by B. D. Malone, et al., Phys. Rev. B **78**, 035210 (2008), and calculated using CASTEP.

3. **Quantification of different ionization channels in surface ablation.**

We have conducted extensive experimental and numerical investigations of plasma production on the surfaces of dielectrics illuminated by intense femtosecond laser pulses. In our experiments, we focused the laser beam on the surface of a transparent dielectric plate and measured transmission of the laser beam through an aperture placed behind the plate, for different values of the incident pulse energy. As the laser fluence was increased but remained under the onset of plasma generation, we observed the effect of self-focusing of the laser beam inside the dielectric with the corresponding growth of transmission through the aperture. At higher fluence, plasma started being generated on the surface through multi-photon and avalanche ionization, counteracting the effect of self-focusing. Correspondingly, the transmission declined.

To numerically model our data, we used a propagation code provided by our long-term collaborator Arnaud Couairon from Ecole Polytechnique in Palaiseau, France. By varying the nonlinear refractive index n_2, and multi-photon and avalanche ionization rate constants α and β,

in the rate equation $\frac{d\rho}{dt} = \alpha I^n + \beta I \rho$, we fitted our data essentially perfectly for different materials including soda-lime glass, fused silica and sapphire. There have been a substantial variability of previously reported data for these constants for glass and fused silica; we are not aware of ionization constants being reported for sapphire. Our experimental data, with fits, are summarized in Figure 4. The corresponding values for ionization constants, together with the values reported previously are listed in the table immediately below the figure. We are currently writing up these results for publication.

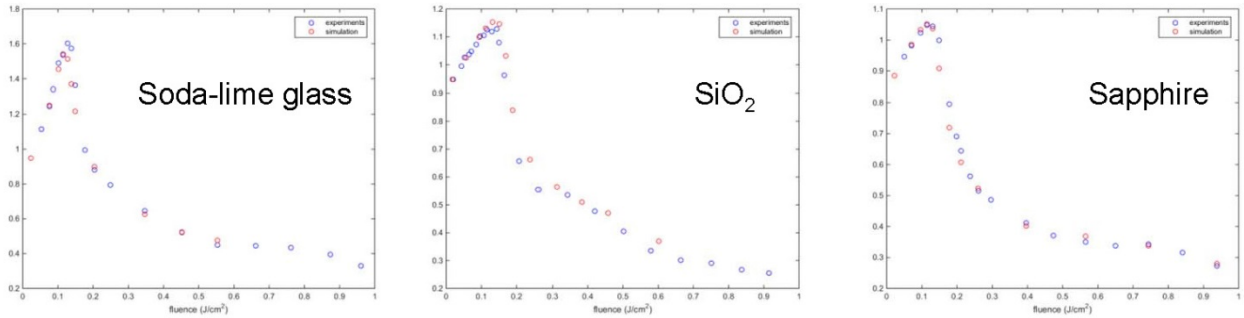

Figure 4: Experimental and numerical data for the transmission of a femtosecond laser pulse through a transparent plate, in the ionization regime, as a function of the incoming beam fluence. Experimental and numerical data points are shown with red and blue circles, respectively. The wavelength of the laser is 800 nm and the pulse duration is 65 fs in all cases. Fitting the data with our model allowed us to extract the values of ionization constants for these materials. These values are shown in the table below.

$$\frac{d\rho}{dt} = \alpha I^n + \beta I \rho$$

Multiphoton Avalanche

Soda-lime: 3 photon @ 800nm
Fused silica: 6 photon @ 800nm
Sapphire: 6 photon @800nm

	Soda-lime	Fused silica	Sapphire
Lenzner, et al, PRL **80**, 4076 (1998)	$\alpha = 7 \times 10^{(-13\pm0.5)} \mathrm{s}^{-1}\mathrm{m}^{-3}(\mathrm{m}^2/\mathrm{W})^3$ $\beta = (1.2 \pm 0.4)\,\mathrm{cm}^2/\mathrm{J}$	$\alpha = 6 \times 10^{(-70\pm0.9)} \mathrm{s}^{-1}\mathrm{m}^{-3}(\mathrm{m}^2/\mathrm{W})^6$ $\beta = (4 \pm 0.6)\,\mathrm{cm}^2/\mathrm{J}$	NA
Li, et al, PRL **82**, 2394 (1999)	$\alpha = 3 \times 10^{-14} \mathrm{s}^{-1}\mathrm{m}^{-3}(\mathrm{m}^2/\mathrm{W})^3$ $\beta = 6\,\mathrm{cm}^2/\mathrm{J}$	$\alpha = 3 \times 10^{(-74)} \mathrm{s}^{-1}\mathrm{m}^{-3}(\mathrm{m}^2/\mathrm{W})^6$ $\beta = (9 \pm 0.6)\,\mathrm{cm}^2/\mathrm{J}$	NA
Our data	$\alpha = (4 \pm 4) \times 10^{-14} \mathrm{s}^{-1}\mathrm{m}^{-3}(\mathrm{m}^2/\mathrm{W})^3$ $\beta = (6 \pm 2)\,\mathrm{cm}^2/\mathrm{J}$	$\alpha = (4 \pm 3) \times 10^{(-66)} \mathrm{s}^{-1}\mathrm{m}^{-3}(\mathrm{m}^2/\mathrm{W})^6$ $\beta = (6 \pm 4)\,\mathrm{cm}^2/\mathrm{J}$	$\alpha = (5 \pm 3) \times 10^{(-65)} \mathrm{s}^{-1}\mathrm{m}^{-3}(\mathrm{m}^2/\mathrm{W})^6$ $\beta = 1 \pm 1\,\mathrm{cm}^2/\mathrm{J}$

Table 1: Values of multiphoton and avalanche constants extracted from fitting our experimental data. Also shown are the values from other sources. Values for sapphire have not been previously available.

4. **First-principle non-paraxial model of energy deposition into a dielectric.**

The development of such a model has been the major goal of this project. While the interaction of femtosecond laser pulses with surfaces of metals and dielectrics has been extensively studied in the past, the interaction of tightly focused laser beams with the bulk of transparent solids and interfaces remains relatively under-explored. This program involved a comprehensive investigation of such an interaction regime. The problem is notoriously difficult from the computational standpoint. A significant absorption of the optical energy occurs only when plasma is formed through multiphoton and avalanche ionization in the otherwise transparent dielectric material. The formed plasma layers swiftly reflect the incident laser beam thus unidirectional or paraxial simplifications are no longer valid. Furthermore, when plasma density grows above the critical value, the thickness of the plasma skin layer becomes significantly sub-wavelength. Therefore in order to properly resolve the plasma volume, the numerical scheme needs to have a very high spatial resolution of the order of several nanometers. For numerical stability, the corresponding temporal resolution needs to be less than one tenth of the optical period. Previously used models were only able to treat cases with weak ionization significantly below the critical value and had relied on various other simplifications. The models used previously generally did not account for the depletion of electron population in the valence band due to ionization and neglected the effects of the band-gap modification resulting from ionization (the band-gap collapse effect). All of those impairments have been corrected in the model developed in this program.

For the simulation of the propagation of a tightly focused femtosecond laser beam inside a transparent dielectric we have developed a comprehensive material response model and coupled it to the (3+1)D FDTD Maxwell solver. The description of ionization takes into account both the instantaneous value of the electric field and the time-averaged light intensity. The dynamics of the created electron cloud is influenced both by the electric field and by electron scattering, which is accounted for by considering both the average (drift) and the chaotic (thermal) electron velocity. It has been shown that all of those features of the model play very important roles in electron dynamics.

The model has been applied to a comprehensive study of the light-plasma dynamics for a wide range of parameters of the incident laser pulse. Our simulations show that the pump field creates a region with plasma density substantially above the critical value, which leads to a strong back-reflection of the incident laser beam. The back-reflected light produces a high-contrast interference pattern with the trailing tail of the forward-propagating pump pulse, which creates several spots of high plasma density prior to the nonlinear focus. During the propagation of the pulse, optical energy is deposited into the lattice by both electron ionization and electron and lattice heating. The deposited energy density can be sufficiently high to evaporate common transparent solids such as fused silica and sapphire. A detailed analysis of the spatiotemporal field profile allowed us to identify a spherical region of high plasma density with localized field oscillations around it. In the Figures 5 and 6 we show examples of the application of the new model to the case of the propagation of tightly focused laser pulses with the durations of 8 fs, 32 fs and 64 fs inside fused silica in the regime of strong ionization. In all cases the peak plasma density is significantly above critical.

An interesting feature that has been made evident by these simulations is the effect of plasmonic enhancement of energy deposition in small plasma structures created on the trailing

edge of the propagating laser pulse. When the size of the small plasma balls evident in Figure 6 is such that the plasmonic resonance frequency for this nanoparticle is near the frequency of the optical driver, the particle starts to resonate with the driving field resulting in the enhancement of energy deposition. This feature can be used for the optimization of material excitation. Another possible way to enhance the deposited energy density is through the use of a bi-chromatic or strongly chirped optical driver. In this case, the temporal front end of the pulse with a lower optical frequency creates plasma structures, while the trailing pulse tail with a higher optical frequency penetrates into these structures and deposits energy in them.

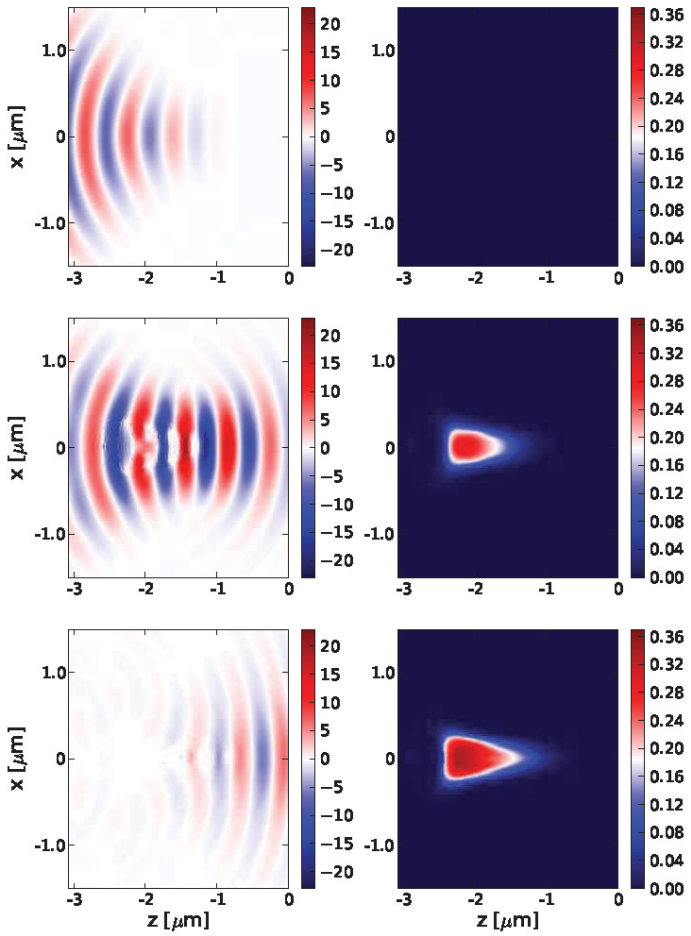

Figure 5: Electric field (left column) and density of conduction-band electrons relative to the density of the SiO_2 molecules (right column). The snapshots are shown at 8 fs before the pulse reaches the focus (top), at the moment when the pulse reaches the focus (middle), and 8 fs after the pulse reaches the focus (bottom). Vacuum intensity that would be achieved at the geometrical focus in the absence of the fused silica sample is 5×10^{14} W/cm^2. The driver pulse has an 800 nm center wavelength and the FWHM pulse duration of 8 fs. The in-vacuum focused spot has a diameter of 0.45 μm.

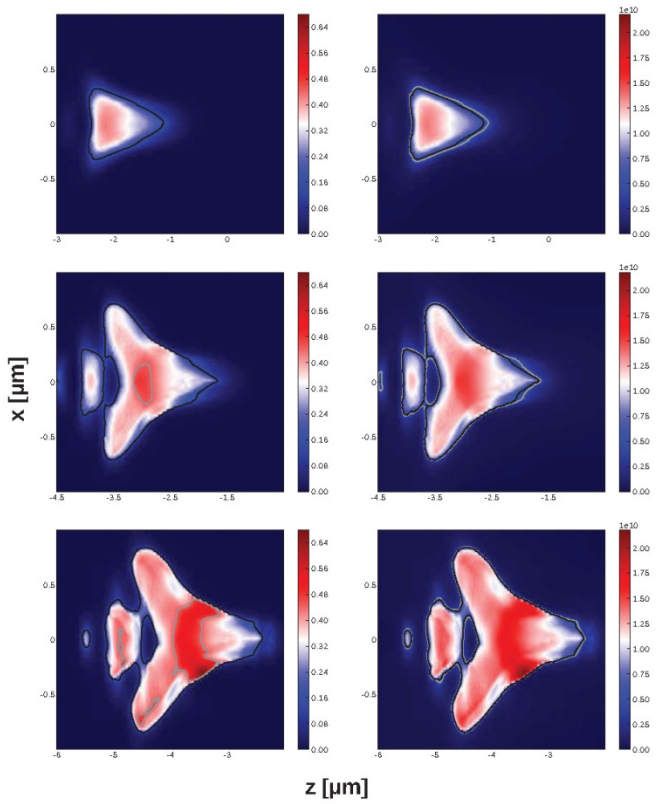

Figure 6: Density of the conduction-band electrons relative to the density of the SiO_2 molecules (left column) and spatial distribution of the deposited energy (right column), both immediately after the passage of the pump pulse. Pulse durations, from top to bottom row, are 8 fs, 32 fs and 64 fs. The peak vacuum intensity is 6×10^{14} in all cases. The remaining parameters are the same as in Figure 5. In the left column, the grey contours encircle the regions where the relative density of plasma exceeds 0.5. (The absolute value of the critical plasma density at 800 nm wavelength is 1.7×10^{21} $1/cm^3$ which corresponds to the relative value of 0.077.) In the right panel, grey and black contours encircle regions where the density of the deposited energy is sufficient to melt and evaporate fused silica, respectively. These two regions are very close to one another indicating a highly nonlinear nature of energy deposition.

5. **Beam and pulse shaping effects in volume laser ablation.**

The investigation of the effects of beam and pulse shaping in volume laser ablation has been the major task of this program. Our results on the in-volume machining with higher order Bessel beams have been discussed in detail in our publications on the subject and in our yearly reports. Here we will discuss our more recent work on the combining Simultaneous Spatial and Temporal focusing (SSTF) with conventional beam shaping (vortex beams), and on using tightly focused SSTF beams in confined microexplosion experiments. The goal of the latter activity has been to enhance the extreme pressure inside the microexplosion void. Both projects are currently being written up for publications.

Most of the applications of laser micromachining rely on ablation of front material surfaces. When machining inside the bulk or on the back surfaces of transparent dielectrics is sought,

spatial and temporal distortions of the laser beam that result from the highly nonlinear propagation of the laser beam through the material may severely impair the fidelity of the machined features. The SSTF approach has been previously shown to reduce the nonlinearity penalty significantly. However, previously SSTF technique has only been used with Gaussian beams. In this program, we have combined the SSTF with conventional beam shaping to generate femtosecond SSTF vortex beams. We have demonstrated the utility of these beam structures by producing single-shot encryptions of doughnut-shaped ablation marks on back surfaces of glass plates. Our experimental setup is schematically shown in Figure 7. Examples of clean doughnut-shaped features produced on the back surface of a glass plate are shown in Figure 8. We point out that no feature could be produced in our experimental geometry by an ordinary vortex beam (without SSTF focusing). As the energy of such a beam is increased, the beam fragments into hot spots and the propagation self-terminates, without the intact, high-intensity beam reaching the back side of the glass plate.

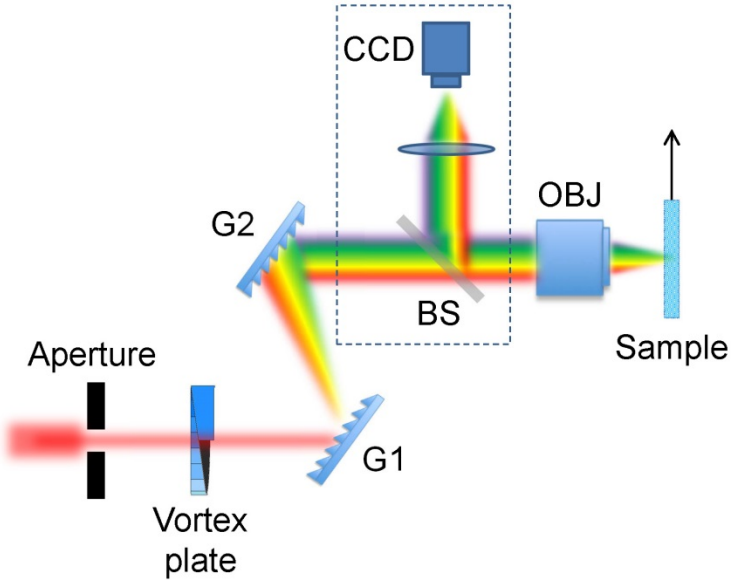

Figure 7: Schematic of the experimental setup. Vortex plate, m=3; G1, G2, blazed gratings, 13 degree blaze angle at wavelength 780 nm with groove density of 600 grooves/mm; BS, beam splitter; Lens, f=10 cm; OBJ, microscope objective NA=0.15

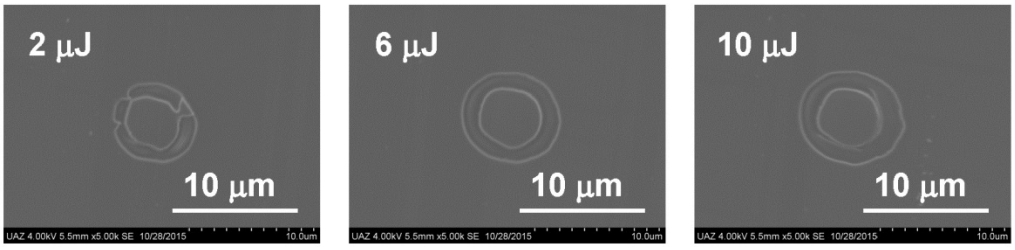

Figure 8: Micromachining structures produced on the back surface of borosilicate glass plate using single-shot SSTF vortex beams. The order of vortex used in our experiments is 3.

We have conducted experiments on the application of SSTF beams to the production of microexplosion voids inside sapphire. The goal has been to enhance the already extreme pressure and temperature conditions that can be achieved inside microexplosions produced by tightly focused ordinary Gaussian beams. We have shown that the application of the SSTF increases the volume of the amorphous region inside the void (where the new super-dense states of matter are located), by about a factor of 3, and increases the maximum pressure by about 50%.

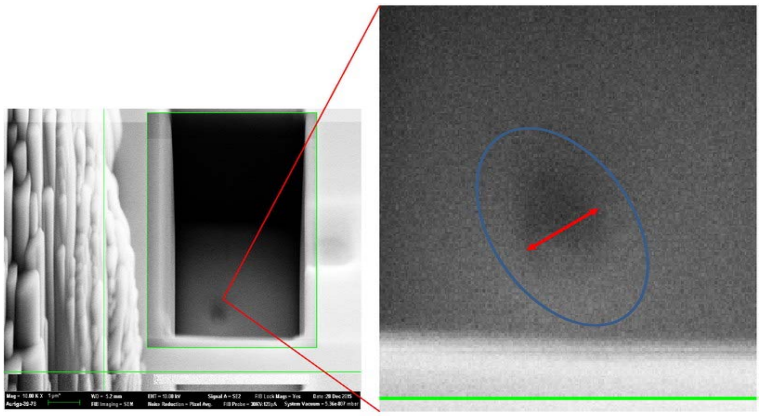

Figure 9: SEM image of the microexplosion void produced inside sapphire by an SSTF beam. The void has been exposed for imaging by focused ion beam milling.

In Figure 9, we show the SEM photograph of the microexplosion void inside sapphire that has been opened using focused ion beam (FIB) milling. We conducted these measurements for different values of input pulse energy, which correspond to different energy densities in the focal volume. The data for the diameters of the amorphous phase of sapphire, that contains microscopic amounts of super-dense aluminum, are shown in Figure 10. As evident from the data, the size of the void obtained by both Gaussian and SSTF beams saturate with energy density. But the SSTF-produced void size saturates at a significantly higher value. The higher void size translates into a higher value of peak pressure inside the void. We estimate that the maximum attainable pressures in the cases of the Gaussian and the SSTF beams are 1.8 TPa and 2.7 TPa, respectively. We are currently writing these results up for publication.

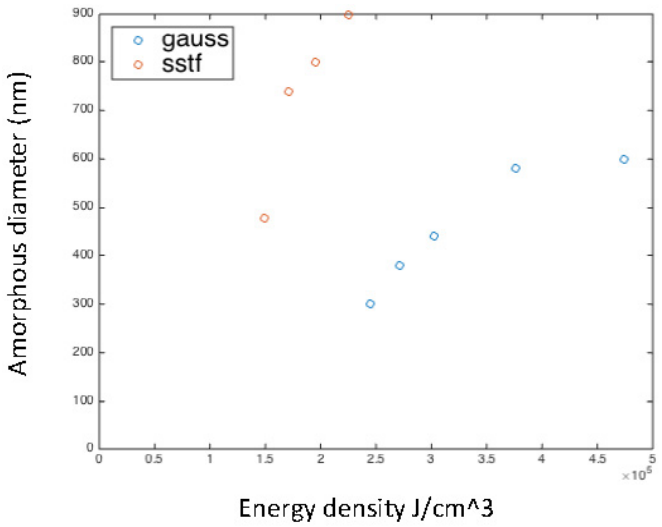

Figure 10: Experimental data for the void size, as a function of the energy density in the focal volume, obtained with Gaussian and with SSTF beams of increasing energy. The size of the void saturates at a much higher value for the case of the SSTF beam.